Springer

Journal of Mechanical Science and Technology 22 (2008) 1889~1895

Journal of
Mechanical
Science and
Technology

www.springerlink.com/content/1738-494x
DOI 10.1007/s12206-008-0728-7

A numerical study on the unsteady flow behavior and the performance of an automotive sirocco fan †

Yohan Jung and Jehyun Baek*

Dept. of Mechanical Engineering, POSTECH, San 31, Hyoja-dong, Pohang 790-784, Korea

(Manuscript Received April 16, 2008; Revised June 25, 2008; Accepted July 23, 2008)

Abstract

An automotive sirocco fan has been widely used in air-conditioning devices. It is essential to understand the flow characteristics of an automotive sirocco fan to satisfy the trends for more efficient and less noise. In this study, numerical calculations were conducted to explain the three-dimensional unsteady, incompressible flow characteristics and performance of the sirocco fan using FLUENT. Reynolds-averaged Navier-Stokes equations with the standard $k-\varepsilon$ turbulence model were used for the numerical analysis. The sliding mesh was used to simulate the relative transient motion of impeller against scroll. It was found that the inactive zone and the secondary flow reduce efficiency because they cause internal losses. A parametric study was performed to improve efficiency of the sirocco fan, using two geometric variables. Reducing the width of impeller could decrease the relative size of inactive zone and secondary flow. Changing the position of cut-off had little influence on the efficiency. Thus an improvement of efficiency could be achieved by reducing the width of impeller.

Keywords: Sirocco fan; Sliding mesh; Width of impeller; Position of cut-off

1. Introduction

A sirocco fan, a kind of centrifugal fan with forward-curved-blade, has been widely used in devices of an automotive HVAC (Heating, Ventilating, and Air Conditioning) system due to relatively high flow rates and low noise. In order to achieve high efficiency, it is necessary to understand flow characteristics of the fan. Many experimental researches have been done on the sirocco fan.

Raj and Swim [1] found that the blade active area depends on the flow rate and the circumferential location of the impeller and there are large flow separation zones near the inlet shroud. Roth [2] performed an experiment to optimize the sirocco fan. His experiments included performance measurements for a series of rotors. Cau et al [3] explained the secondary flow patterns observed in the scroll by applying the simplified secondary flow theory and found that flow rate variation produces different secondary flow patterns. Kind and Tobin [4] measured mean velocity, flow direction, and total pressure inside and outside the rotor by using a five-hole prove. Humbad et al [5] found that an important factor of noise is the flow separation at the cut-off. Because of the complexity of the fan geometry, it is not easy to know detailed information about the flow field of the fan by an experiment. However, CFD study can predict the complicated fluid behavior in detail. Fischer [6] performed the three-dimensional flow computations for one blade and compared with the experiment results. Gronier et al [7], using STAR-CD, performed the three-dimensional computations.

In this study, the three-dimensional unsteady, incompressible turbulent flow calculations were con-

† This paper was presented at the 9th Asian International Conference on Fluid Machinery (AICFM9), Jeju, Korea, October 16-19, 2007.

*Corresponding author. Tel.: +82 54 279 2168, Fax.: +82 54 279 3199
E-mail address: jhback@postech.ac.kr

Table 1. Geometric data for the sirocco fan.

Parameter	Size
d_1	120 mm
d_2	145 mm
d_1 / d_2	0.83
Z	44
b	70.3 mm
W	92 mm
θ_c	21.4º
α	7º
β_1	80º
β_2	150º
t	1.8

ducted using FLEUNT and a parametric study was performed to improve efficiency of the sirocco fan, using two geometric variables, such as width of impeller and location of cut-off.

2. Numerical methods

Governing equations for unsteady incompressible turbulent flows are the continuity and Reynolds-averaged Navier-Stokes equations. These equations are as follows:

$$\frac{\partial \rho}{\partial t} + \frac{\partial}{\partial x_i}(\rho u_i) = 0 \tag{1}$$

$$\frac{\partial}{\partial t}(\rho u_i) + \frac{\partial}{\partial x_j}(\rho u_i u_j) = -\frac{\partial p}{\partial x_i} + \frac{\partial}{\partial x_j}\left[\mu\left(\frac{\partial u_i}{\partial x_j} + \frac{\partial u_j}{\partial x_i} - \frac{2}{3}\delta_{ij}\frac{\partial u_l}{\partial xl}\right)\right] + \frac{\partial}{\partial x_j}(-\rho\overline{u_i' u_j'}) \tag{2}$$

where u_i and u_i' are mean and fluctuating velocities, respectively. Governing equations were solved with a standard $k-\varepsilon$ turbulence model. A central-difference scheme was used for the diffusion terms while a first-order upwind difference scheme was used for the convection terms. The SIMPLE algorithm was used to match pressure and velocities. For the inlet condition, the uniform mass flow on the inlet surface was applied. For the outlet condition, the static pressure on the outlet surface was applied. On the wall of the blades and scroll, no-slip conditions were imposed for the velocity components. In this study, there are two grid systems. One is the rotating grid system of the impeller. The other is the stationary grid system of the scroll. The sliding mesh technique was employed at the interface of two grid systems to transfer of the flow variables.

Table 2. Calculation conditions.

Parameter	Value
Flow coefficient	0.24
Inlet mass flow rate	0.0748 kg/s
Outlet static pressure	101384.5 Pa
Rotating speed	2000 rpm

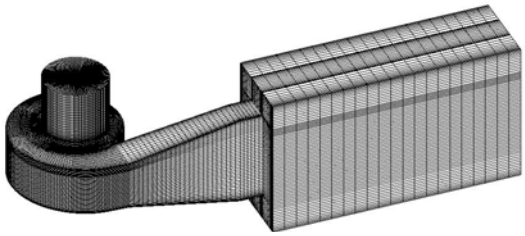

(a) Total

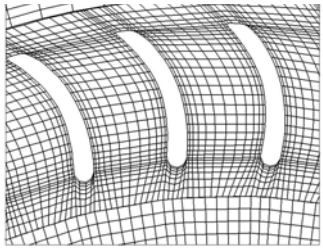

(b) Blades

Fig. 1. Computational grids.

Detailed geometric data for the sirocco fan are shown in Table 1. Based on the geometry, a multi-block hexahedral mesh was generated using ICEM-CFD. The total computational grid system is shown in Fig. 1(a). The rotating part has 814,000 nodes and the stationary part has 430,739 nodes. So the total has 1,244,739 nodes. A detailed view of grids near the blade is shown Fig. 1(b).

3. Results and discussions

3.1 Flow characteristics

The simulation was conducted at ϕ=0.24 and the rotational speed of the rotor was 2000rpm. The detailed calculation conditions are summarized in Table 2. The computation was continued until the rotor made ten revolutions. To validate the accuracy of the

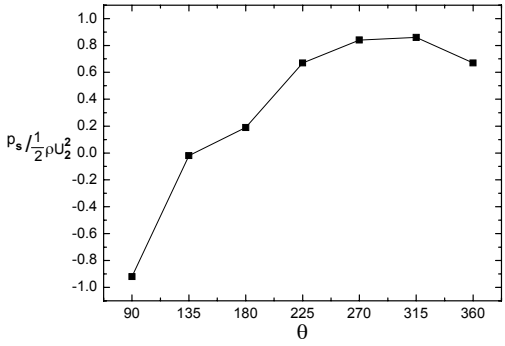

(a) Kim et al.

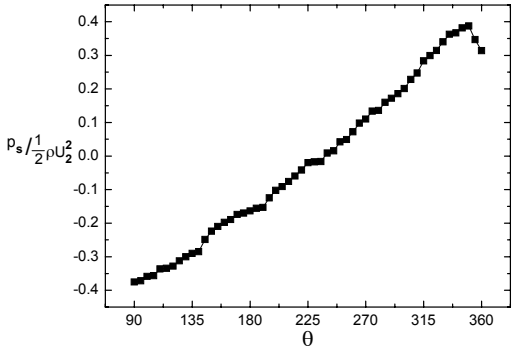

(b) Calculation

Fig. 2. Characteristics of static pressure distribution along the scroll wall on the mid-span.

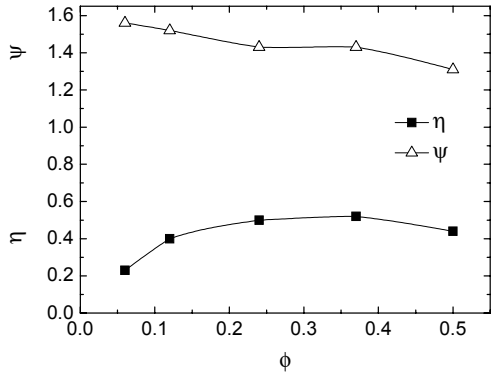

Fig. 3. Performance curve.

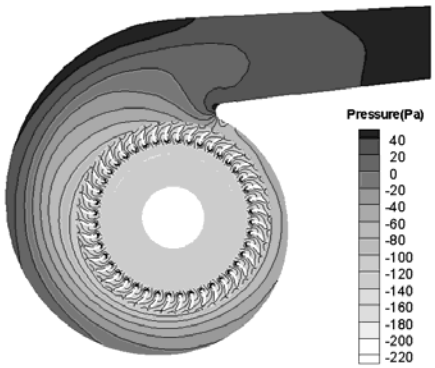

Fig. 4. Time-averaged static pressure contours at mid-span plane.

numerical result, the static pressure distribution along the scroll wall on the mid-span was presented with another case of experimental that of Kim et al [8] in Fig. 2. Both results represent that the static pressure increases as a scroll angle does. The curves shown in Fig. 3 were plotted with the efficiency and total pressure coefficient versus the flow coefficient in order to investigate performance of the sirocco fan. Efficiency is almost the maximum at the design point and the total pressure coefficient decreases as the flow coefficient increases. The time-averaged static pressure fields at the mid-span plane were shown in Fig. 4. As shown in this figure, pressure is higher at the scroll wall side than at the inside of the rotor and it changes in the circumferential direction. It is known that the flow separation zones, called inactive zones, are a significant cause of the efficiency reduction. Instantaneous radial velocity contours at the blade exit plane (i.e., $\theta - Z$ plane) are shown in Fig. 5. There are large flow separation zones near the shroud plane while flows are well passing through the impeller near the hub plane. Especially, the flow separation zones are dominant near the cut-off region ($\theta = 21.4^0$). In the scroll, strong three-dimensional flows exist. Fig. 6 shows the secondary flow formation on cross-sections in the scroll at a scroll angle 90^0, 180^0, 270^0, 360^0 by the velocity vectors and static pressure contours. In this figure, 'S' represents the scroll side wall while 'B' represents the blade side. The upper line means the shroud side while the lower line means the hub side. The static pressure contours are averaged by one blade pitch time. As shown in this figure, the static pressure gradually increases from the blade side to the scroll wall side and two vortices govern the secondary flow on all cross-sections. The upper vortex, clockwise rotating vortex, is shown entirely in cross-sections of the scroll while the lower vortex, counter-clockwise rotating vortex, is shown at the lower scroll wall. Also, this figure represents that a center of the upper vortex moves from the blade side to the scroll wall side as a scroll angle increases.

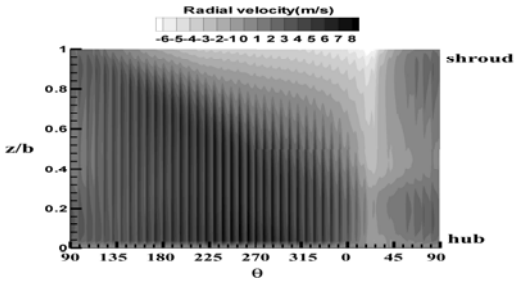

Fig. 5. Instantaneous radial velocity contours at the blade exit plane.

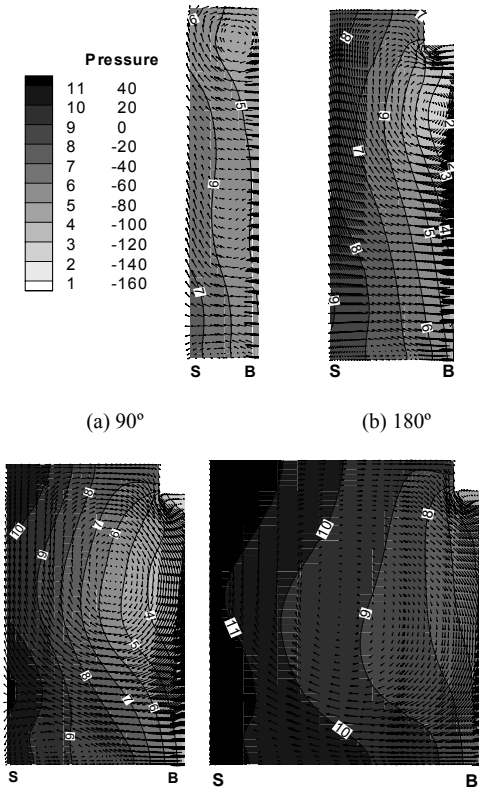

(a) 90º (b) 180º

(c) 270º (d) 360º

Fig. 6. Secondary flow vectors on cross-sections in the scroll.

3.2 Parametric study

It is known that the width of impeller, one of main design parameters of the sirocco fan, has influence on the efficiency. In this study, we investigated the relation of flow characteristics and the impeller width change. b/d_2 was used as a non-dimensional coefficient of the impeller width. Calculations were conducted for the impeller width of b/d_2 = 0.48, 0.43, 0.31. Fig. 7 shows comparisons of efficiency due to changes in the width of impeller. It is found in Fig. 7 that efficiency increases as the width of impeller reduces in the low flow rate regions, but reverses in the high flow rate regions. Compared with efficiency for the impeller width of b/d_2 = 0.48 at the design point (ϕ = 0.24), efficiency is increased by 2, 4% for the impeller width of b/d_2 = 0.43, 0.31, respectively. The total pressure coefficient for the impeller width of b/d_2 = 0.31 is rapidly decreased in the high flow rate regions, while the total pressure coefficient for the impeller width of b/d_2 = 0.43 is slightly decreased.

Table 3. Comparisons of inactive zones at the blade exit plane due to changes in width of impeller.

	$A(m^2)$	$A_I(m^2)$	A_I / A (%)
b/d_2 = 0.48	0.0329	0.0066	20.1
b/d_2 = 0.43	0.0290	0.0047	16.2
b/d_2 = 0.31	0.0207	0.0019	9.2

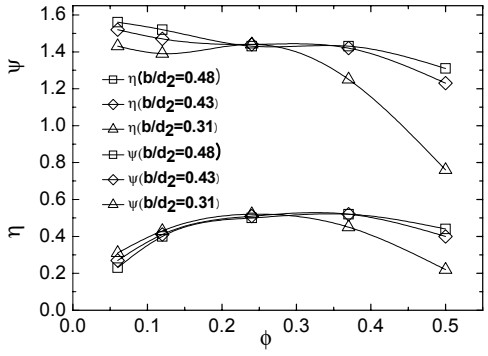

Fig. 7. Comparisons of efficiency curves due to changes in width of impeller.

In order to find the reason for the efficiency improvement, the relative extent of inactive zones through the impeller was investigated at the blade exit plane. As shown in Table 3, the reduction of impeller width decreases the relative extent of inactive zones from 20.1% to 16.2%, 9.2% of the total blade exit plane area. Fig. 8(a), (b), (c) shows instantaneous radial velocity contours at the blade exit plane for the impeller of width b/d_2 = 0.48, 0.43, 0.31, respectively. It reveals that as the impeller width reduces, the negative radial velocity regions decrease, meaning that flows are successfully passing through the blades. Especially, the flow separation zones near the cut-off region ($\theta = 21.4^0$) which is a major cause of energy loss is decreased by reducing the impeller width.

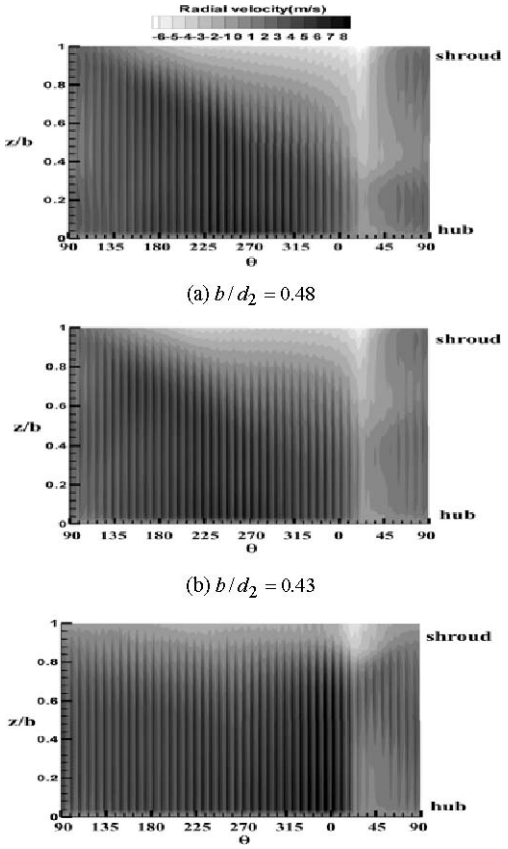

(a) $b/d_2 = 0.48$

(b) $b/d_2 = 0.43$

(c) $b/d_2 = 0.31$

Fig. 8. Comparisons of radial velocity contours at the blade exit plane.

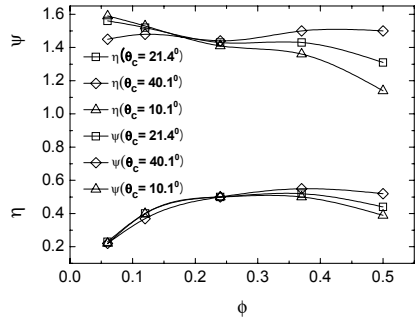

Fig. 9. Comparisons of performance curves due to changes in cut-off.

The strong secondary flow in the scroll is another important cause to decrease the efficiency, because the vortex caused by secondary flows induces the inner loss. In order to obtain the secondary flow strength due to changes in the width of impeller, the circulations (Γ) on cross-sections in the scroll were evaluated. Table 4 shows comparisons of the circulations between $b/d_2 = 0.48$ and $b/d_2 = 0.43$ on a scroll cross-section at a scroll angle 90^0, 180^0, 270^0, 360^0. The positive circulations (Γ^+) and the negative circulations (Γ^-) are presented in the Table 4. The positive circulations mean the strength of counter-clockwise rotating vortices while the negative circulations mean the strength of clockwise rotating vortices. As shown in the Table 4, it is found that the circulations are decreased by reducing the impeller width. Table 5 shows comparisons of the circulations between $b/d_2 = 0.48$ and $b/d_2 = 0.31$. Compared with the circulation reduction in the case of Table 4, the circulation reduction in the case of Table 5 is larger.

Table 4. Comparisons of circulations between $b/d_2 = 0.48$ and $b/d_2 = 0.43$.

Scroll angle		$b/d_2 = 0.48$	$b/d_2 = 0.43$	Reduction(%)
90^0	Γ^+	0.09	0.08	11.11
	Γ^-	-0.35	-0.31	11.43
180^0	Γ^+	0.37	0.35	5.41
	Γ^-	-0.78	-0.71	8.97
270^0	Γ^+	0.53	0.51	3.77
	Γ^-	-1.23	-1.06	13.82
360^0	Γ^+	0.59	0.57	3.39
	Γ^-	-1.29	-1.10	14.73

Table 5. Comparisons of circulations between $b/d_2 = 0.48$ and $b/d_2 = 0.31$.

Scroll angle		$b/d_2 = 0.48$	$b/d_2 = 0.31$	Reduction(%)
90^0	Γ^+	0.09	0.09	0
	Γ^-	-0.35	-0.02	37.14
180^0	Γ^+	0.37	0.29	21.62
	Γ^-	-0.78	-0.52	33.33.
270^0	Γ^+	0.53	0.46	13.21
	Γ^-	-1.23	-0.72	41.46
360^0	Γ^+	0.59	0.66	-10.61
	Γ^-	-1.29	-1.02	20.93

The position of cut-off is another important design parameter of the sirocco fan. Another parametric study was performed by changing the cut-off position. To investigate the effect on flow fields due to changes in cut-off position, calculations were conducted for the cut-off position of $\theta_c = 21.4^0, 40.1^0, 10.1^0$. Fig. 9 shows comparisons of performance curves due to changes in cut-off position. For the three cases, the efficiency is almost same at the design point. However, the sirocco fan for the cut-off position of $\theta_c = 40.1^0$ has almost constant total pressure coeffi-

Table 6. Comparisons of inactive zones at the blade exit plane due to changes in cut-off position.

	$A(m^2)$	$A_I(m^2)$	$A_I/A(\%)$
$\theta_c = 21.4^0$	0.0329	0.0066	20.1
$\theta_c = 40.1^0$	0.0329	0.0074	21.4
$\theta_c = 10.1^0$	0.0329	0.0060	18.5

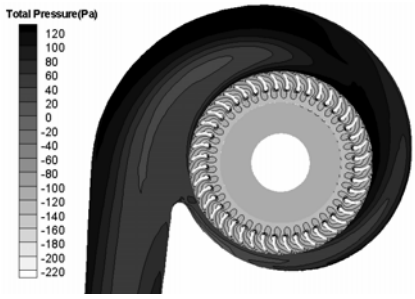

(a) $\theta_c = 21.4$º

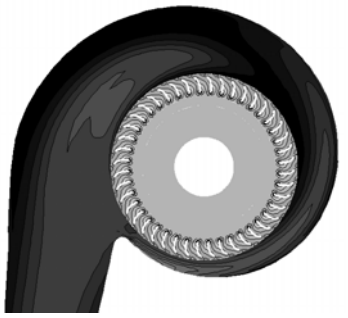

(b) $\theta_c = 40.1$º

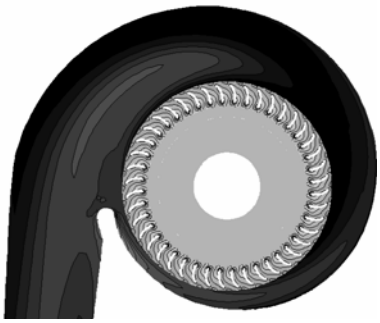

(c) $\theta_c = 10.1$º

Fig. 10. Comparisons of time-averaged total pressure contour at mid span plane.

cient in the overall flow rate regions. It reveals that the sirocco fan has wide operating range. Table 6 shows comparisons of inactive zones at the blade exit plane due to changes in cut-off position. As shown in Table 6, there is no great difference in the extent of inactive zones. Fig. 10 shows comparisons of time-averaged total pressure contour at mid span plane. Also, there is no great difference in energy loss as shown in Fig. 10.

4. Conclusions

To improve the efficiency of the sirocco fan, parametric studies were performed using two geometric variables, such as the width of impeller and the location of cut-off. At the design point, the efficiency was increased by 2% and 4% for the impeller width of $b/d_2 = 0.43$ and 0.31 respectively. In case of $b/d_2 = 0.31$, large energy loss was generated in the high flow rate regions. The efficiency for $b/d_2 = 0.43$ was improved at the design point not having any large energy loss at the overall operating range. The position of the cut-off had little influence on the efficiency. However, in case of $\theta_c = 40.1^0$, the total pressure coefficient was almost constant in the overall operating range. It means that the sirocco fan of $\theta_c = 40.1^0$ has more wide operating range that the original one.

Acknowledgments

This study has been supported by the KATECH (Korea Automotive Technology Institute) under the contract 10023799

Nomenclature

A_I : Inactive flow area
b : Width of impeller
d_1, d_2 : Inner and outer diameter of impeller, respectively
t : Blade thickness
W : Width of scroll
Z : Number of blades

Greek

α : Expansion angle of scroll
β_1 , β_2 : Blade inlet and outlet angle, respectively
ϕ : Flow coefficient
Γ : Circulation
η : Efficiency
θ , θ_c : Angle of scroll and cut-off, respectively
ρ : Density
ψ : Total pressure coefficient

References

[1] D. Raj and W. B. Swim, Measurements of the mean flow velocity and velocity fluctuations at the exit of an FC centrifugal fan rotor, *Journal of Engineering for Gas Turbines Power,* 106 (1981) 906-912.

[2] H. W. Roth, Optimierung von trommelläufer-ventilatoren, *Strömungsmechanik und Strömung-smaschi-nen*, 29 (1981) 1-45.

[3] G. Cau and N. Mandas, Measurement of primary and secondary flows in an industrial forward-curved centrifugal fan, *Journal of Fluids Engineering,* 109 (1987) 353-358.

[4] R. J. Kind and M. G. Tobin, Flow in a centrifugal fan of the squirrel-cage type, *Journal of Turbo machinery,* 112 (1990) 84-90.

[5] N. G. Humbad and T. J. Hall, Case study on reducing automotive blower rumble noise, Proc. of the ASME, Noise and Control Division, Nca-Vol. 22, (1996) 233-242.

[6] D. Fischer, Airflow simulation through automotive blowers using computational fluid dynamics, SAE 950438 (1995).

[7] P. Gronier and P. Gilotte, Airflow Simulation of an Automotive Blower for a HVAC Unit, SAE 960961 (1996).

[8] Y. C. Kim and S. H. Lee, Experimental Study for Reduction of Blade Passing Frequency Noise Level of Multi-Blade Fan, Society of Air-Conditioning and Refrigerating Engineers of Korea, (1997).